

Sensitivity of flexural and torsional vibration modes of atomic force microscope cantilevers to surface stiffness variations

Joseph A Turner and Joshua S Wiehn

Department of Engineering Mechanics, W317.4 Nebraska Hall, University of Nebraska—Lincoln, Lincoln, NE 68588-0526, USA

Received 8 February 2001, in final form 29 June 2001

Published 28 August 2001

Online at stacks.iop.org/Nano/12/322

Abstract

Dynamic modes of atomic-force microscopy offer new possibilities for imaging because of the availability of the various vibrational modes of the probes. However, each mode has a different sensitivity to variations in surface stiffness. This sensitivity directly controls the image contrast. Low-stiffness cantilevers have typically been unusable for imaging of stiff materials because of the lack of sensitivity of the first flexural mode. In this paper, the sensitivities of the flexural and torsional modes are derived. Closed-form expressions are obtained for cantilevers with constant cross sections. For cantilevers with other shapes, an approximate solution is developed using the method of Rayleigh–Ritz. The interaction of the cantilever with the surface is modelled by linear springs, which restricts the results to experiments involving low-amplitude excitations. Both flexural and torsional vibration modes are considered. For given nominal values of surface and AFM probe properties, the appropriate mode for highest contrast may be predicted.

1. Introduction

The atomic force microscope (AFM) was originally developed to provide surface topography information [1]. The deflection of the microscope cantilever plotted as a function of surface location gives a high-resolution image of surfaces. Recent applications of the AFM have exploited the dynamic characteristics of the AFM. Many versions of dynamic atomic force microscopy have been proposed for imaging specimens [2–6]. All of these methods rely on the relative motion between the AFM tip and the specimen surface. This work has shown that high-frequency excitation of the specimen surface or AFM cantilever can provide a better signal-to-noise ratio for imaging while doing less damage to the specimen surface. These techniques also offer the potential for high-resolution measurement of material properties and surface properties [2, 3, 7, 8]. These techniques utilize the dynamical response of the cantilever, specifically in terms of the higher-order vibrational modes. The dynamical response of an elastic cantilevered beam in contact with a surface, however, is not

easily described. The tip–sample interaction forces are, in general, nonlinear and are the subject of intensive research themselves. When an elastic beam interacts with these surface forces, the many flexural and torsional modes must be included as part of the complete dynamics. These higher modes are often excited simultaneously in experiments. In much of the current research, the amplitude of the surface motion is kept small. In this case, the motion may be studied by linearizing the nonlinear tip–sample interaction forces about an equilibrium point. The linearized motion is much easier to analyse, although it does not describe all possible cantilever motion. If the motion is very large, the nonlinear motion may be chaotic [9].

It was recently shown that the surface interactions acting through the cantilever tip affect each of the vibration modes differently [10, 11]. The effects of the surface stiffness and damping act locally at the position on the beam at which the tip is attached. Because each mode has a different mode shape, each mode is affected by the local surface loading in a different way. Each mode was also seen to have a different sensitivity

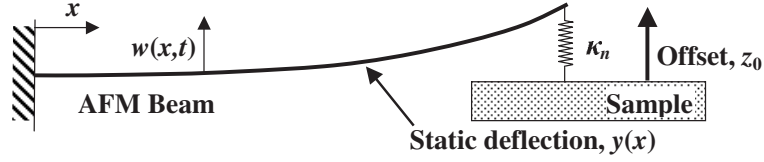


Figure 1. Schematic diagram of the flexural vibration problem. The AFM probe is in contact with a specimen. Initial contact is made when the sample offset, z_0 , is zero. The static sample offset causes a static beam deflection, $y(x)$. The dynamic motion, $w(x, t)$, is defined relative to $y(x)$. The contact force between the tip and sample is modelled as a linear spring with stiffness κ_n .

to local variations in stiffness or damping [2, 10, 12]. The most sensitive modes are those which should be used for imaging because their response will provide the highest contrast.

In this paper, the linear dynamics of AFM cantilevers are considered in terms of both flexural and torsional vibrations. The flexural and torsional models used here are restricted to beams which are much longer than their width. When this condition is not satisfied, plate theory is more accurate [13]. Exact expressions for the modal sensitivities are derived for cantilevers with uniform cross sections. The sensitivity defines the relative change in the frequency of a mode due to changes in surface stiffness. An approximate solution technique is then developed for cantilevers with nonuniform cross sections. This technique, based on the Rayleigh–Ritz method, results in an expression for the sensitivities in terms of the approximate eigenvalue problem (EVP). The approximate method is validated using the exact expressions derived for cantilevers with uniform cross sections. Sample results for triangular cantilevers are also presented using the derived approximate solution. It is anticipated that the derived sensitivities, exact and approximate, will improve the understanding of image contrast and materials characterization in AFM research.

2. Flexural vibrations

The primary type of cantilever deflection for most AFM studies is flexural. If the sample surface is vibrated normal to the surface, the AFM probe will vibrate flexurally. The flexural AFM modes have been studied extensively since it was first recognized that the AFM behaves as a continuous member with appropriate modes [14].

2.1. Linear theoretical model

A uniform, homogenous beam of constant, rectangular cross section is cantilevered at one end as depicted in figure 1. At the end opposite to the cantilever, a tip with a small radius is attached. The linearized boundary value problem for this system has a governing equation and boundary conditions given by [10, 13]

$$EI \frac{\partial^4 w(x, t)}{\partial x^4} + \rho A \frac{\partial^2 w(x, t)}{\partial t^2} = 0, \quad (1)$$

$$w(x, t)|_{x=0} = 0, \quad w'(x, t)|_{x=0} = 0, \quad (2)$$

$$w''(x, t)|_{x=L} = 0, \quad EI w'''(x, t)|_{x=L} = \kappa_n w(x, t)|_{x=L}. \quad (3)$$

In equations (1)–(3), $w(x, t)$ defines the cantilever position relative to its initial static deflection, $y(x)$. The AFM

cantilever is defined by E , the modulus of the cantilever, I , the area moment of the cantilever, ρ , the volume density, and A , the cross-sectional area of the cantilever. Here, EI and ρA are assumed uniform over the length of the cantilever. The boundary conditions given by equation (2) correspond to conditions of zero displacement and zero slope at $x = 0$. The boundary conditions given by equation (3) correspond to zero moment at $x = L$ and the force balance between the beam and the linear tip–sample stiffness. Because a linear model is used to describe the tip–sample interaction force, the results are restricted to small tip displacements. The actual value of the linear spring constant, κ_n , in terms of the tip and sample parameters depends on the interaction model used. Simple Hertzian theory [15, 16], more complex Maugis mechanics [16] or other models [17–20] may all be linearized about some initial equilibrium position to determine this spring constant.

Equations (1)–(3) define completely the linearized flexural vibration problem. The natural frequencies of the cantilever vibrations are dependent on the linear spring constant. These frequencies are found through derivation of the corresponding eigenvalue problem. We seek harmonic solutions of the form $w(x, t) = W(x)e^{i\omega t}$. Substitution into equations (1)–(3) gives the EVP in the form of a fourth-order ordinary differential equation (ODE) and four boundary conditions. The solution of the eigenvalue problem gives the mode shape [10]

$$W(x) = D(\sin kx - \sinh kx - D_0(\cos kx - \cosh kx)), \quad (4)$$

where k is the flexural wavenumber and

$$D_0 = \frac{\sin kL + \sinh kL}{\cos kL + \cosh kL}. \quad (5)$$

In equation (4), D defines the amplitude of the mode shape. The linearized eigenvalue problem does not depend on this amplitude. The mode shape given by equation (4) has been written to satisfy directly the boundary conditions of displacement and slope (equations (2)) and that of zero moment at $x = L$ (the first of equations (3)).

The characteristic equation defines the wavenumbers which admit solutions to the problem. The characteristic equation is found by substituting equation (4) into the boundary condition involving the linear spring. The characteristic equation is given by [10, 14]

$$C(\gamma, \beta_n) \equiv \gamma^3(\cos \gamma \cosh \gamma + 1) - \beta_n(\sinh \gamma \cos \gamma - \sin \gamma \cosh \gamma) = 0, \quad (6)$$

where $\gamma = kL$ is the normalized wavenumber and $\beta_n = \kappa_n/(EI/L^3)$ is the normal contact stiffness relative to the stiffness of the cantilever. Equation (6) is also used to define the characteristic function $C(\gamma, \beta_n)$ which will be used below.

The dispersion relation between wave number and frequency is found by substituting the mode shape equation (4) into the EVP. This relation is given by

$$f^2 = \frac{EI}{4\pi^2 \rho AL^4} \gamma^4. \quad (7)$$

The linear vibration model is appropriate when the specimen amplitude is kept small while remaining in contact with the AFM tip. The linear vibrations are used for current materials characterization studies [2, 3, 7, 8]. It should be noted that additional factors have been omitted from the above model. The tip position, tip mass and initial angle of the AFM cantilever have all been neglected. The inclusion of these parameters follows in a straightforward manner [11].

2.2. Sensitivity

The characteristic equation given by equation (6) defines the wavenumbers in terms of β_n . Allowable frequencies are governed by the zeros of the characteristic function, equation (6). The interest here is in the modes which will change significantly for small variations of stiffness across the sample. Thus, we are indirectly interested in the change of γ with respect to β_n . Differentiation of equation (6) with respect to β_n implies that

$$\frac{d\gamma}{d\beta_n} = -\frac{\partial C / \partial \beta_n}{\partial C / \partial \gamma}. \quad (8)$$

Equation (6) gives

$$\begin{aligned} \frac{d\gamma}{d\beta_n} &= (\cos \gamma \sinh \gamma - \sin \gamma \cosh \gamma) \\ &\times \{3\gamma^2(1 + \cos \gamma \cosh \gamma) + 2\beta_n \sin \gamma \sinh \gamma \\ &+ \gamma^3(\cos \gamma \sinh \gamma - \sin \gamma \cosh \gamma)\}^{-1}. \end{aligned} \quad (9)$$

Equation (9) is the wave number sensitivity to changes in surface stiffness. Of course, experimentally it is the change in frequency f that is measured. Further expansion gives

$$\frac{\partial f}{\partial \beta_n} = \frac{\partial f}{\partial \gamma} \frac{d\gamma}{d\beta_n}. \quad (10)$$

The dispersion relation, equation (7) implies that

$$\frac{\partial f}{\partial \gamma} = \gamma \frac{1}{\pi} \sqrt{\frac{EI}{\rho AL^4}}. \quad (11)$$

Finally, the expression for the shift in frequency due to surface stiffness changes is

$$\begin{aligned} \frac{df}{d\beta_n} &= \frac{1}{2\pi} \sqrt{\frac{EI}{\rho AL^4}} (2\gamma(\cos \gamma \sinh \gamma - \sin \gamma \cosh \gamma) \\ &\times \{3\gamma^2(1 + \cos \gamma \cosh \gamma) \\ &+ \gamma^3(\cos \gamma \sinh \gamma - \sin \gamma \cosh \gamma) \\ &+ 2\beta_n(\sin \gamma \sinh \gamma)\}^{-1}. \end{aligned} \quad (12)$$

For a given normal stiffness, β_n , the frequency equation, equation (6) is solved for the wavenumbers. The corresponding sensitivities for each mode may then be calculated using equation (12).

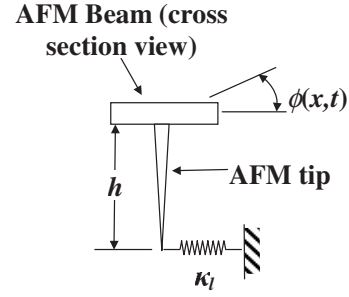


Figure 2. End view of the torsional problem. The AFM probe is in contact with a specimen. The contact is modelled as a linear lateral spring with stiffness κ_l , which acts at the end of the AFM tip. The dynamic torsional motion is described by the twist angle, $\phi(x, t)$.

A dimensionless form of the flexural sensitivity is given by

$$\sigma_f = \frac{df/d\beta_n}{\frac{1}{2\pi} \sqrt{\frac{EI}{\rho AL^4}}}. \quad (13)$$

This form of the sensitivity may be thought of as the ratio of the measurement frequency resolution, $df/d\beta_n$, relative to a characteristic frequency of the cantilever, $\frac{1}{2\pi} \sqrt{\frac{EI}{\rho AL^4}}$. Example results of equation (13) are presented below.

3. Torsional vibrations

A similar sensitivity analysis may also be developed when considering the torsional modes. In this section, the sensitivities of the torsional modes to variations in lateral stiffness are derived for a uniform cross section cantilever. The schematic diagram in figure 2 shows the boundary condition assumed at the AFM tip. The contact of the tip with the sample is modelled with a linear lateral spring.

3.1. Linear theoretical model

Let the parameter $\phi(x, t)$ be defined as the twist of the bar, which is a function of position along the beam x and time t . The torsional vibrations of a uniform bar are described by [13]

$$\left(\frac{G\xi}{\rho J}\right) \frac{\partial^2 \phi(x, t)}{\partial x^2} = \frac{\partial^2 \phi(x, t)}{\partial t^2}, \quad (14)$$

where G is the shear modulus, J is the polar moment of area and ρ is the mass density. The parameter ξ in equation (14) is a torsional constant related to the cross-sectional area. For a rectangular cross section with width b and thickness t , this constant is given by [21]

$$\xi = \frac{1}{3} t^4 \left(\frac{b}{t} - 0.630\right). \quad (15)$$

Equation (15) is an approximation based on the assumption that the cross section is a narrow rectangle with $b > t$. This assumption is valid for most AFM cantilevers. The exact expression for ξ , written as a series solution, is found in elasticity texts [21].

The required boundary conditions are given by

$$\phi(x = 0, t) = 0, \quad (16)$$

$$G\xi \left. \frac{\partial \phi(x, t)}{\partial x} \right|_{x=L} = -\kappa_1 h^2 \phi(L, t), \quad (17)$$

where h is the tip height as illustrated by figure 2. Equation (16) is the condition of no rotation at $x = 0$. Equation (17) is the moment balance at $x = L$ with κ_1 the lateral spring stiffness which is assumed to be linear. It is related to the sample shear rigidity [15, 16].

Looking for harmonic solutions of the form $\phi(x, t) = \Phi(x)e^{i\omega t}$, gives the eigenvalue problem. The solution for $\phi(x)$ is given by [13]

$$\Phi(x) = C_1 \sin px, \quad (18)$$

where the torsional wavenumber p is related to frequency ω through the dispersion relation

$$p = \omega \sqrt{\frac{\rho J}{G\xi}}. \quad (19)$$

The second boundary condition, equation (17), gives the characteristic equation

$$C(\gamma, \beta_1) \equiv \gamma \cos \gamma + \beta_1 \sin \gamma = 0, \quad (20)$$

where $\gamma = pL$ is the normalized torsional wavenumber. The parameter $\beta_1 = \kappa_1 h^2 L / G\xi$ defines the lateral stiffness of the surface relative to the torsional rigidity of the beam ($G\xi/L$). As was seen in the flexural case, the characteristic equation is the basis for determining the modal sensitivities.

3.2. Sensitivity

The torsional characteristic function $C(\gamma, \beta_1)$, defined by equation (20) defines the torsional wave numbers in terms of the normalized lateral stiffness. The interest is in the modes which will change significantly for small variations of lateral stiffness across the sample. Following the same procedure as for the flexural modes we find the torsional modal sensitivity

$$\frac{\partial f}{\partial \beta_1} = \frac{1}{2\pi} \sqrt{\frac{G\xi}{\rho J L^2}} \frac{\sin \gamma}{\gamma \sin \gamma - (1 + \beta_1) \cos \gamma}, \quad (21)$$

or in normalized form

$$\sigma_t = \frac{\partial f / \partial \beta_1}{\frac{1}{2\pi} \sqrt{\frac{G\xi}{\rho J L^2}}}. \quad (22)$$

The torsional sensitivity, equation (22), is defined in a similar manner as the flexural. It is the ratio of the measurement frequency resolution, $df/d\beta_n$, relative to a characteristic frequency of the cantilever, $\frac{1}{2\pi} \sqrt{\frac{G\xi}{\rho J L^2}}$. Example results of equation (22) are also presented below.

4. Approximate methods

The above analysis for both the flexural and torsional sensitivities was done under the assumption of a uniform cross section. However, many cantilevers commonly used in AFM research do not have a uniform cross section. For these cantilevers, the bending stiffness EI , linear mass density ρA ,

torsional stiffness $G\xi$ and the polar moment per unit length ρJ are all functions of position along the cantilever. The V-shaped cantilever is just one example. In this section, the method of Rayleigh–Ritz is used to approximate the natural frequencies. Subsequently, an expression for the modal sensitivities to surface stiffness is then derived. The exact solutions derived above for flexural and torsional vibrations also serve to validate the approximate methods derived in this section.

The Rayleigh–Ritz method is fundamentally based on Rayleigh’s quotient [13]. The governing partial differential equations for the flexural and torsional vibrations have eigenvalue problems which may be represented by

$$\mathcal{L}[\psi_r] = \omega_r^2 \mathcal{M}[\psi_r], \quad (23)$$

where \mathcal{L} and \mathcal{M} are linear operators on eigenfunction ψ_r with corresponding frequency ω_r . Operator \mathcal{L} is of even order ($2q$) for flexure and torsion. The eigenfunctions must satisfy all boundary conditions of the problem. If we multiply both sides of the eigenvalue problem by ψ_r and integrate over the domain Ω of the system, we obtain

$$\omega_r^2 = \frac{\int_{\Omega} \psi_r \mathcal{L}[\psi_r] d\Omega}{\int_{\Omega} \psi_r \mathcal{M}[\psi_r] d\Omega} = \frac{N[\psi_r]}{D[\psi_r]}, \quad (24)$$

for $r = 1, 2, \dots$. Equation (24) defines the numerator $N[\psi]$ and denominator $D[\psi]$ of Rayleigh’s quotient, $R[\psi] = N[\psi]/D[\psi]$.

Rayleigh’s quotient forms the basis for the method of Rayleigh–Ritz. A set of admissible functions u is defined as being q times differentiable over the domain of the system. These functions are also required to satisfy the geometric boundary conditions, but need not satisfy the natural boundary conditions. The eigenfunctions, ψ_r , are then expanded in terms of the admissible functions as

$$\psi_r(x) = \sum_{i=1}^r a_i u_i(x). \quad (25)$$

The stationarity of Rayleigh’s quotient is then exploited by attempting to minimize the ratio in equation (24). The minimization procedure results in a discretized eigenvalue problem [13]

$$K\mathbf{a} = \lambda^2 M\mathbf{a}, \quad (26)$$

where $\mathbf{a} = \{a_1, a_2, \dots, a_r\}^T$. This eigenvector has components which are the coefficients of the expansion, equation (25), for the r th eigenfunction, $\psi_r(x)$. The eigenvalue in equation (26), λ^2 , is the approximation of the exact eigenvalue, ω^2 . The stiffness and mass matrices in equation (26) are defined in terms of the admissible functions and operators by

$$K_{ij} = \int_{\Omega} u_i \mathcal{L}[u_j] d\Omega, \quad (27)$$

$$M_{ij} = \int_{\Omega} u_i \mathcal{M}[u_j] d\Omega. \quad (28)$$

These expressions for the Rayleigh–Ritz method are now applied to the flexural and torsional problems.

4.1. Flexural vibrations

The necessary operators for the flexural vibrations of a nonuniform beam are given by [13]

$$\mathcal{L}[\psi] = \frac{\partial^2}{\partial x^2} \left[EI(x) \frac{\partial^2 \psi(x)}{\partial x^2} \right], \quad (29)$$

$$\mathcal{M}[\psi] = \rho A(x) \psi(x). \quad (30)$$

In terms of the admissible functions, $u_i(x)$, the numerator of Rayleigh's quotient for flexure is

$$N[u] = \int_{\Omega} u \mathcal{L}[u] d\Omega = \int_0^L u \frac{\partial^2}{\partial x^2} (EI(x) u'') dx. \quad (31)$$

Integrating equation (31) by parts twice gives

$$N[u] = \kappa_n u^2(L) + \int_0^L EI(x) (u'')^2 dx. \quad (32)$$

The denominator reduces to

$$D[u] = \int_{\Omega} u \mathcal{M}[u] d\Omega = \int_0^L \rho A(x) (u)^2 dx. \quad (33)$$

The components of the mass and stiffness matrices are then defined as

$$K_{ij} = \int_0^L EI(x) \left(\frac{d^2 u_i(x)}{dx^2} \right) \left(\frac{d^2 u_j(x)}{dx^2} \right) dx + \kappa_n u_i(L) u_j(L), \quad (34)$$

$$M_{ij} = \int_0^L \rho A(x) u_i(x) u_j(x) dx. \quad (35)$$

These matrices may be normalized for comparison with the exact results derived in section 2. In this case,

$$\begin{aligned} \tilde{K}_{ij} &= \frac{K_{ij}}{EI_0/L^3} = \int_0^1 \frac{EI(\tilde{x})}{EI_0} \left(\frac{d^2 u_i(\tilde{x})}{d\tilde{x}^2} \right) \\ &\times \left(\frac{d^2 u_j(\tilde{x})}{d\tilde{x}^2} \right) d\tilde{x} + \beta_n u_i(1) u_j(1), \end{aligned} \quad (36)$$

$$\tilde{M}_{ij} = \frac{M_{ij}}{\rho A_0 L} = \int_0^1 \frac{\rho A(\tilde{x})}{\rho A_0} u_i(\tilde{x}) u_j(\tilde{x}) d\tilde{x}, \quad (37)$$

where EI_0 and ρA_0 are the bending stiffness and mass density at $x = 0$, respectively, $\beta_n = \kappa_n / (EI_0/L^3)$ and $\tilde{x} = x/L$. Note that in equation (36), the tip has been assumed to be at the end of the beam.

In terms of the normalized matrices, $\tilde{\mathbf{K}}$ and $\tilde{\mathbf{M}}$, the eigenvalue problem is given by

$$\tilde{\mathbf{K}} \mathbf{a} = \Omega^2 \tilde{\mathbf{M}} \mathbf{a}, \quad (38)$$

where \mathbf{a} is the eigenvector of expansion coefficients and the normalized frequency is

$$\Omega = \frac{\lambda}{\sqrt{EI_0/\rho A_0 L^4}}. \quad (39)$$

The derivative of the eigenvalue problem, equation (38), is then taken with respect to β_n . The result is

$$\frac{\partial \tilde{\mathbf{K}}}{\partial \beta_n} \mathbf{a} + \tilde{\mathbf{K}} \frac{\partial \mathbf{a}}{\partial \beta_n} = 2\Omega \frac{\partial \Omega}{\partial \beta_n} \tilde{\mathbf{M}} \mathbf{a} + \Omega^2 \frac{\partial \tilde{\mathbf{M}}}{\partial \beta_n} \mathbf{a} + \Omega^2 \tilde{\mathbf{M}} \frac{\partial \mathbf{a}}{\partial \beta_n}. \quad (40)$$

Equation (40) is then simplified. First, we see that the mass matrix, $\tilde{\mathbf{M}}$, does not depend explicitly on β_n . We then assume that the change in the eigenvector to small changes in stiffness is negligible. Equation (40) then simplifies to

$$\frac{\partial \tilde{\mathbf{K}}}{\partial \beta_n} \mathbf{a} = 2\Omega \frac{\partial \Omega}{\partial \beta_n} \tilde{\mathbf{M}} \mathbf{a}. \quad (41)$$

Finally, we multiply on the left by \mathbf{a}^T . The normalization condition

$$\mathbf{a}^T \tilde{\mathbf{M}} \mathbf{a} = 1, \quad (42)$$

is used to simplify the sensitivity to surface stiffness. The final result is the approximate form of the flexural sensitivity

$$\sigma_f = \frac{\partial \Omega}{\partial \beta_n} = \frac{1}{2\Omega} \mathbf{a}^T \frac{\partial \tilde{\mathbf{K}}}{\partial \beta_n} \mathbf{a}. \quad (43)$$

This expression for the modal sensitivity relies on information from the eigenvalue problem, equation (38). For a given stiffness, β_n , the eigenvalues, Ω , and eigenvectors, \mathbf{a} , are found from equation (38). The sensitivity for each mode for the same stiffness is then found directly using equation (43). The approximate solution may be compared with the above exact solution, equation (13). The exact result was derived assuming a constant cross section. In this case, $EI(\tilde{x})/EI_0 = 1$, and $\rho A(\tilde{x})/\rho A_0 = 1$.

4.2. Torsional vibrations

The necessary operators for torsional vibrations of a nonuniform beam are given by

$$\mathcal{L}[\psi] = \frac{\partial}{\partial x} \left[G\xi(x) \frac{\partial \psi(x)}{\partial x} \right], \quad (44)$$

$$\mathcal{M}[\psi] = \rho J(x) \psi(x). \quad (45)$$

In terms of the admissible functions, $u_i(x)$, the numerator of Rayleigh's quotient for torsion reduces to

$$N[u] = \kappa_1 h^2 u^2(L) + \int_0^L G\xi(x) (u')^2 dx. \quad (46)$$

The denominator is given by

$$D[u] = \int_{\Omega} u \mathcal{M}[u] d\Omega = \int_0^L \rho J(x) (u)^2 dx. \quad (47)$$

The components of the mass and stiffness matrices are then defined as

$$K_{ij} = \int_0^L G\xi(x) \left(\frac{du_i(x)}{dx} \right) \left(\frac{du_j(x)}{dx} \right) dx + \kappa_1 h^2 u_i(L) u_j(L), \quad (48)$$

$$M_{ij} = \int_0^L \rho J(x) u_i(x) u_j(x) dx. \quad (49)$$

These matrices are normalized for comparison with the exact results. In this case,

$$\begin{aligned} \tilde{K}_{ij} &= \frac{K_{ij}}{G\xi_0/L} = \int_0^1 \frac{G\xi(\tilde{x})}{G\xi_0} \left(\frac{du_i(\tilde{x})}{d\tilde{x}} \right) \\ &\times \left(\frac{du_j(\tilde{x})}{d\tilde{x}} \right) d\tilde{x} + \beta_1 u_i(1) u_j(1), \end{aligned} \quad (50)$$

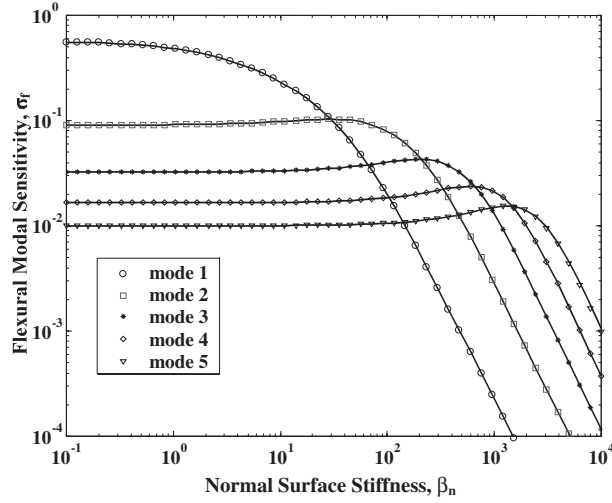


Figure 3. Exact and approximate expressions for flexural modal sensitivity, σ_f , for a cantilever with uniform cross section. The solid curves are the exact solution (equation (13)) and the symbols are the approximate solution from equation (43). The approximate solution is based on a ten-term polynomial expansion.

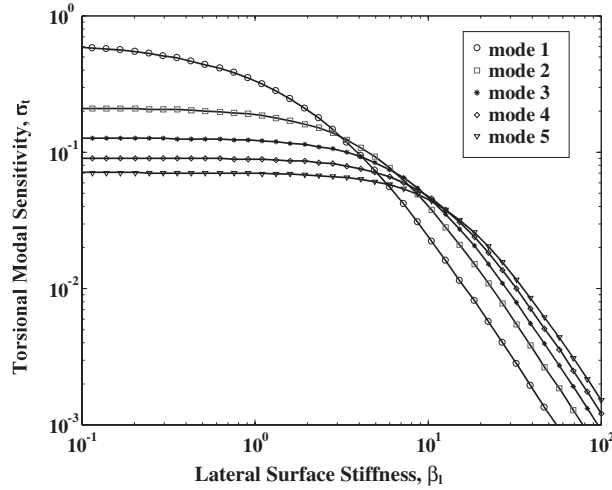


Figure 4. Exact and approximate expressions for torsional modal sensitivity, σ_t , for a cantilever with uniform cross section. The solid curves are the exact solution (equation (22)) and the symbols are the approximate solution from equation (54). The approximate solution is based on a ten-term polynomial expansion.

$$\tilde{M}_{ij} = \frac{M_{ij}}{\rho J_0 L} = \int_0^1 \frac{\rho J(\tilde{x})}{\rho J_0} u_i(\tilde{x}) u_j(\tilde{x}) d\tilde{x}, \quad (51)$$

where $G\xi_0 = G\xi(0)$ and $\rho J_0 = \rho J(0)$ are the torsional stiffness and polar mass moment at $x = 0$, respectively, $\beta_l = \kappa_1 h^2 L / G\xi_0$ and $\tilde{x} = x/L$.

In terms of the normalized matrices, $\tilde{\mathbf{K}}$ and $\tilde{\mathbf{M}}$, the eigenvalue problem is given by

$$\tilde{\mathbf{K}} \mathbf{a} = \Omega^2 \tilde{\mathbf{M}} \mathbf{a}, \quad (52)$$

where \mathbf{a} is the eigenvector of expansion coefficients and the normalized frequency is

$$\Omega = \frac{\lambda}{\sqrt{G\xi_0 / \rho J_0 L^2}}. \quad (53)$$

Following the same procedure as for the flexural modes, we find the approximate torsional modal sensitivity

$$\sigma_t = \frac{\partial \Omega}{\partial \beta_l} = \frac{1}{2\Omega} \mathbf{a}^T \frac{\partial \tilde{\mathbf{K}}}{\partial \beta_l} \mathbf{a}. \quad (54)$$

5. Results

Several results are now presented based on the exact (equations (13) and (22)) and approximate results (equations (43) and (54)) derived above. First, results for cantilevers with uniform cross sections are presented using both the exact solution and the approximate solution. Then, results for a cantilever with nonuniform cross section are presented.

5.1. Uniform cross section

The flexural sensitivity, σ_f , of the first five modes is plotted in figure 3 for the case of a constant cross section beam. The exact results are shown as the solid curves and the approximate results are shown as the symbols. The exact and the approximate flexural sensitivities agree very well. Several conclusions may be reached from this figure. When the cantilever is much more compliant than the sample surface, the first mode is most sensitive to changes in surface stiffness.

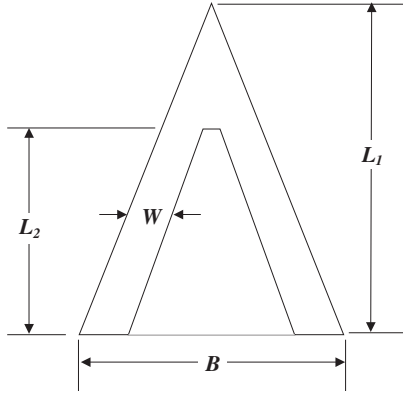


Figure 5. Geometry of the cantilever with nonuniform cross section used in the example calculations.

The highest value of σ_f for all modes is found from the limit of $\beta_n \rightarrow 0$ of equation (13). In this limit, the wavenumbers approach those for the free vibration problem (i.e. $\gamma_1 = 1.8751$, $\gamma_2 = 4.694$, $\gamma_3 = 7.854$ etc). Thus the maximum sensitivities for the first three modes are $\sigma_f = 0.57$, 0.091 and 0.032 . We also see the effect of a stiff sample on the sensitivity. When β_n is greater than about 30, the sensitivity of the first mode becomes smaller than that of the second mode. Thus, we expect that the second mode will experience the largest shifts in frequency of all of the modes. At the same time, we see that the overall sensitivity for all modes has been reduced to a maximum around 0.1. When the stiffness ratio, β_n is about 160, the first mode is less sensitive than modes two through five. The sensitivity of all modes scales with $1/\beta_n^2$ for large β_n .

The approximate solution shown in figure 3 requires a choice of admissible functions, $u_i(x)$. These functions must be sufficiently differentiable over the domain of the system and they must satisfy the geometric boundary conditions. Recommended functions include polynomials or the mode shapes from the exact solution, equation (4). The results shown in figure 3 are based on admissible functions $u_i(\bar{x}) = (\frac{x}{L})^{i+1}$.

The number of expansion functions used in equation (25) must be chosen with care. If too few are used, the approximation of the natural frequencies is poor. On the other hand, high-order polynomials may create numerical instabilities, such that a large number of terms should not be used. A reasonable compromise has been found to be ten functions. With this number, the estimate of the first five frequencies is quite good and numerical instabilities are not encountered. The results shown in figure 3 were calculated using a ten-term polynomial expansion. The error between the two solutions is less than 0.02% for modes 1–4 with the largest error in the highest mode. The error for mode 5 is less than 1% for $\beta_n < 2(10)^3$, with a maximum error of 7% for $\beta_n = 10^4$.

From a practical standpoint, figure 3 may be used as in the following example. Consider an AFM probe with rectangular cross section (width = $40 \mu\text{m}$, thickness = $2 \mu\text{m}$, $L = 200 \mu\text{m}$). For a given set of cantilever properties ($E = 170 \text{ GPa}$, $I = 24.7 \times 10^{-24} \text{ m}^4$, $\rho = 2330 \text{ kg m}^{-3}$), we find that $\frac{1}{2\pi} \sqrt{\frac{EI}{\rho AL^4}} = 19.6 \text{ kHz}$. If the measurement frequency resolution is $df/d\beta_n = 0.5 \text{ kHz}$, the flexural sensitivity of the

measurement system is $\sigma_f = 0.026$. If this value is plotted on figure 3 as a horizontal line, the ‘usable’ modes for imaging stiffness variations are then clear. For this example, only the first three modes would lie above this line, and only for $\beta_n < 1000$.

The torsional modal sensitivity for a cantilever with a uniform cross section is plotted in figure 4 for the first five modes. The sensitivity is plotted versus normalized lateral stiffness with β_1 ranging from 0.01 to 100. The exact results are shown as the solid curves, while the approximation is shown by the symbols. The torsional modal sensitivity has many similar features to the flexural. The first mode is the most sensitive for smaller values of β_1 . In the limit of small β_1 the maximum sensitivity for the first mode is 0.5. For stiffer samples, the sensitivity begins to decrease, finally dropping like $1/\beta_1$ for large β_1 . In contrast with the flexural sensitivity, we see that the torsional sensitivities are more compact—the sensitivity of the modes is about the same for $\beta_1 > 4$. The transition region for the torsional sensitivity occurs at about the same level of lateral stiffness for all modes.

The approximate solution for torsional vibrations was calculated using a ten-term polynomial expansion with polynomials $u_i(\bar{x}) = (\frac{x}{L})^i$. The exact and the approximate torsional sensitivities agree very well. The two solutions are virtually identical using the ten-term polynomial expansion. The error between the two solutions is less than 0.021% for modes 1–4 with the largest error in the highest mode. The error for mode 5 is less than 0.65% for the entire range of β_n .

5.2. Nonuniform cross section

The approximate solution is also used to examine the flexural sensitivity for a nonuniform cross section. Consider the cantilever shown in figure 5 with a triangular plan view and thickness t . Calculations were done using the approximate sensitivity formulae of equations (43) and (54). A ten-term polynomial expansion was used for both the flexural and torsional sensitivities with the same polynomial functions as in section 5.1. Values for the geometric properties ($L_1 = 200 \mu\text{m}$, $L_2 = 145 \mu\text{m}$, $B = 164 \mu\text{m}$, $W = 20 \mu\text{m}$, $t = 0.6 \mu\text{m}$) and material properties ($E = 179 \text{ GPa}$, $\nu = 0.28$, $\rho = 2330 \text{ kg m}^{-3}$) were chosen to be similar to typical AFM beams.

The flexural modal sensitivity for this triangular cantilever is shown in figure 6 for the first five modes. The curves in this figure are similar to those shown in figure 3 for the uniform cross section. There are, however, several distinct differences between the two sets of curves. First, we see that the sensitivities are not as well separated as in the uniform case. For example, the sensitivity of the third mode is about 17.5 times smaller than the first for the uniform cantilever. For the triangular, this same ratio is only about 4.3. Thus, the higher modes for the triangular cantilever are much more usable than those of a uniform beam. Because the sensitivities are more closely spaced, we also see that the value of the surface stiffness is smaller when the first mode sensitivity is equal to that of the second. For the uniform beam, this occurs at $\beta_n \approx 30$ while for the triangular it occurs at $\beta_n \approx 12$. Another difference between the triangular and uniform cantilever is the value of stiffness at which the sensitivity begins the steep decent. For

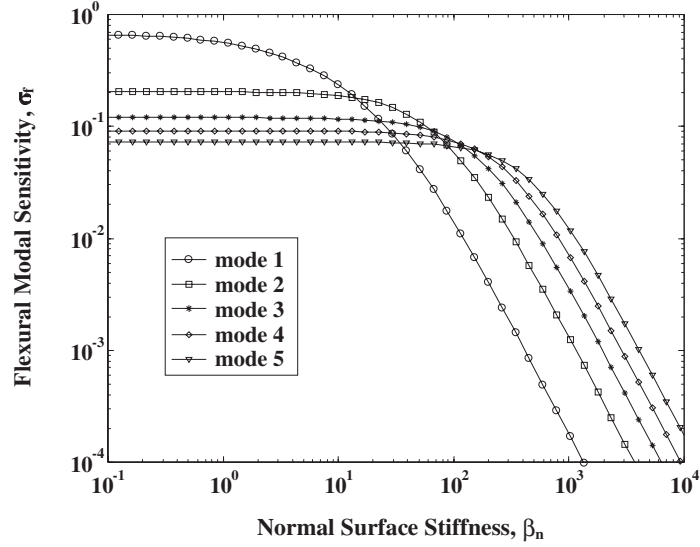


Figure 6. Flexural modal sensitivity, σ_f , for the triangular cantilever shown in figure 5 with $L_1 = 200 \mu\text{m}$, $L_2 = 145 \mu\text{m}$, $B = 164 \mu\text{m}$, $W = 20 \mu\text{m}$, thickness $t = 0.6 \mu\text{m}$ and material properties $E = 179 \text{ GPa}$, $\nu = 0.28$ and $\rho = 2330 \text{ kg m}^{-3}$.

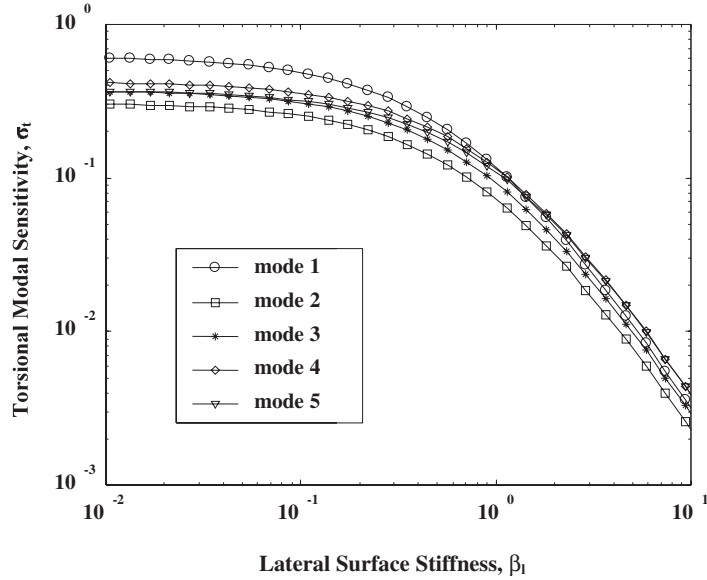


Figure 7. Torsional modal sensitivity, σ_t , for the triangular cantilever shown in figure 5 with $L_1 = 200 \mu\text{m}$, $L_2 = 145 \mu\text{m}$, $B = 164 \mu\text{m}$, $W = 20 \mu\text{m}$, thickness $t = 0.6 \mu\text{m}$ and material properties $E = 179 \text{ GPa}$, $\nu = 0.28$ and $\rho = 2330 \text{ kg m}^{-3}$.

the triangular beam sensitivities, this transition occurs around $\beta_n \approx 100$, much less than for the uniform beam. Thus, the overall sensitivity of the triangular cantilever is greater than or equal to that of the uniform beam for $\beta_n < 100$, but the flexural sensitivity of the triangular beam is less than the uniform for $\beta_n > 100$.

The torsional modal sensitivity for this same triangular cantilever is shown in figure 7 for the first five modes. The results are very different from those for the uniform cross section shown in figure 4. It should be noted that the range of lateral stiffness differs between figures 4 and 7. The sensitivities for the triangular cantilever are much closer to each other for all values of lateral stiffness. However, they decrease more quickly than in figure 4 for increasing stiffness. The most interesting result seen in figure 7 is the ordering of the sensitivities, which is nonintuitive. The first mode is the most

sensitive for low β_l as might be expected. However, the second mode is the least sensitive of the first five modes. The shape of the cantilever can impact the modal sensitivity considerably.

6. Discussion

The flexural and torsional vibrations of AFM cantilevers have been discussed in this paper. In particular, the sensitivities of the modes to changes in surface stiffness have been examined. For cantilevers with uniform cross sections, exact expressions for the sensitivities were derived. As expected, the results showed that the first mode is the most sensitive for materials that are compliant relative to the cantilever. It was also shown that higher-order vibration modes may be more sensitive than the first if the surface stiffness is high enough.

An approximate form for the sensitivities was also derived based on the method of Rayleigh–Ritz. Results were presented which validated the exact expressions. In addition, modal sensitivity results were presented for a triangular cantilever as an example of a cantilever with nonuniform cross section. The flexural sensitivities were more closely spaced than those for the uniform cantilever. The sensitivity of the higher modes was also seen to begin decreasing for a lower value of surface stiffness than for the uniform cross section cantilever. The approximate form of sensitivity is also important for design of new cantilevers. Using the approximate formulae, predictions of modal sensitivity may be made such that cantilevers with optimum sensitivity are created for specified uses.

In addition, the expressions for the sensitivities, both exact and approximate, are simple enough that they lend themselves to on-line computations. The frequency and sensitivity expressions discussed in this paper have been developed into on-line computational tools (<http://em-jaturner.unl.edu/calcs.htm>). The user enters AFM cantilever data into an html form. The data are then used to calculate the modal frequencies and sensitivities as a function of normal or lateral surface stiffness. The results are posted graphically or in table format. The table data may be copied by the user into a spreadsheet or other data analysis program. The authors anticipate that such tools will be of great value to the general AFM community.

Acknowledgments

This work was sponsored by the Air Force Office of Scientific Research under grant no F49620-99-1-0254. The views and conclusions contained herein are those of the authors and should not be interpreted as necessarily representing the official policies or endorsements, either expressed or implied, of the Air Force Office of Scientific Research or the US Government. Support of the Center for Electro-Optics at the University of Nebraska—Lincoln is also gratefully acknowledged.

References

- [1] Binning G, Quate C F and Gerber C 1986 Atomic force microscope *Phys. Rev. Lett.* **56** 930–3
- [2] Rabe U, Amelio S, Kester E, Scherer V, Hirsekorn S and Arnold W 2000 Quantitative determination of contact stiffness using atomic force acoustic microscopy *Ultrasonics* **38** 430–7
- [3] Dinelli F, Biswas S K, Briggs G A D and Kolosov O V 2000 Measurements of stiff-material compliance on the nanoscale using ultrasonic force microscopy *Phys. Rev. B* **61** 13995–14006
- [4] Yamanaka K, Noguchi A, Tsuji T, Koike T and Goto T 1999 Quantitative material characterization by ultrasonic AFM *Surf. Interface Anal.* **27** 600–6
- [5] Stark R W, Drobek T and Heckl W M 1999 Tapping-mode atomic microscopy and phase-imaging in higher eigenmodes *Appl. Phys. Lett.* **74** 3296–8
- [6] Inagaki K, Kolosov O V, Briggs G A D and Wright O B 2000 Waveguide ultrasonic force microscopy at 60 MHz *Appl. Phys. Lett.* **76** 1836–8
- [7] Yamanaka K, Tsuji T, Noguchi A, Koike T and Mihara T 2000 Nanoscale elasticity measurement with *in situ* tip shape estimation in atomic force microscopy *Rev. Sci. Instrum.* **71** 2403–8
- [8] Yalalioglu G G, Degertekin F L, Crozier K B and Quate C F 2000 Contact stiffness of layered materials for ultrasonic atomic force microscopy *J. Appl. Phys.* **87** 7491–6
- [9] Burnham N A, Kulik A J, Gremaud G and Briggs G A D 1995 Nanosubharmonics: the dynamics of small nonlinear contacts *Phys. Rev. Lett.* **74** 5092–5
- [10] Turner J A, Hirsekorn S, Rabe U and Arnold W 1997 High-frequency response of atomic-force microscope cantilevers *J. Appl. Phys.* **82** 966–79
- [11] Rabe U, Turner J and Arnold W 1998 Analysis of the high-frequency response of atomic-force microscope cantilevers *Appl. Phys. A* **66** S277–82
- [12] Drobek T, Stark R W, Gräber M and Heckl W M 1999 Overtone atomic force microscopy studies of decagonal quasicrystal surfaces *New J. Phys.* **1** 15.1–15.11
- [13] Meirovitch L 1967 *Analytical Methods in Vibrations* (New York: Macmillan)
- [14] Rabe U, Janser K and Arnold W 1996 Vibrations of free and surface-coupled atomic force microscope cantilevers: theory and experiment *Rev. Sci. Instrum.* **67** 3281–93
- [15] Johnson K L 1985 *Contact Mechanics* (Cambridge: Cambridge University Press)
- [16] Maugis D 2000 *Contact, Adhesion and Rupture of Elastic Solids* (Berlin: Springer)
- [17] Hirsekorn S, Rabe U and Arnold W 1997 Theoretical description of the transfer of vibrations from a sample to the cantilever of an atomic force microscope *Nanotechnology* **8** 57–66
- [18] Fogden A and White L R 1990 Contact elasticity in the presence of capillary condensation *J. Colloid Interface Sci.* **138** 414–30
- [19] Derjaguin B V, Muller V M and Toporov Y P 1975 Effect of contact deformations on the adhesion of particles *J. Colloid Interface Sci.* **53** 314–26
- [20] Johnson J L, Kendall K and Roberts A D 1971 Surface energy and the contact of elastic solids *Proc. R. Soc. A* **324** 301–13
- [21] Timoshenko S P and Goodier J N 1987 *Theory of Elasticity* (New York: McGraw-Hill)